Front. Earth Sci. 2023, 17(2): 487–504
https://doi.org/10.1007/s11707-022-1024-z

RESEARCH ARTICLE

Sedimentary characteristics of lacustrine deep-water gravity flow in the third member of Paleogene Shahejie Formation in Dongying Sag, Bohai Bay Basin, China

Yuanpei ZHANG[1], Chuanhua LI[3], Xuecai ZHANG[3], Xuqing FANG[3], Yong WANG[3], Jinliang ZHANG[4], Jun XIE[1,2], Jinkai WANG (✉)[1,2]

1 College of Earth Science and Engineering, Shandong University of Science and Technology, Qingdao 266590, China
2 Laboratory for Marine Mineral Resources, Qingdao National Laboratory for Marine Science and Technology, Qingdao 266237, China
3 Sinopec Shengli Oilfield Co., Dongying 257000, China
4 Faculty of Geographical Science, Beijing Normal University, Beijing 100875, China

© Higher Education Press 2023

Abstract Many types of sedimentary systems occur in the middle of the third member of the Shahejie Formation ($E_2S_3^2$) of the Paleogene in the Dongying Sag east of the Bohai Bay Basin. Due to the topography and material supply, traction and gravity flow depositions are intertwined in this area, and the sand body types are complex and diverse, making it challenging to improve the accuracy of their description and prediction and restricting oil reservoir exploration and development. Therefore, this paper documents our systematic study of the sedimentary characteristics of the southern slope of Dongying Depression, the formation mechanism of different sand body types, and the prediction of sand body distribution. First, according to the coring well's single-well facies and vertical rock sequence, nine single lithofacies types and five lithofacies association types were identified. Combined with the well logging facies marks of all wells, the depositional models of delta and gravity flow depositional systems were established in the study area. Then, the gravity flow was divided into slip, collapse, debris flow, and turbidity flow according to its development mechanism. Finally, the distribution law of the gravity flow sedimentary facies type was predicted. Gravity flow sliding deposits are primarily distributed near the delta front, slump and clastic flow deposits are distributed near the far slope, and turbidity current deposits are distributed at the far slope. With the gradual shrinkage of the water body in the north-west direction and the continuous advancement of the river delta, the gravity flow sand body gradually disappears in the late $E_2S_3^2$ and transits to delta plain deposition.

Received May 20, 2022; accepted October 23, 2022

E-mail: wangjk@sdust.edu.cn

Keywords Dongying Sag, gravity flow, sedimentary characteristics, Bohai Bay Basin

1 Introduction

Forel (1885) discovered that large amounts of suspended matter carried by the Rhone River into Lake Geneva were deposited not in shallow water but deep-water, which he called specific gravity flow. Then, the "graded bedding is a sign of turbidity current", was proposed, laying a foundation for studying gravity flow sedimentation (Kuenen and Migliorini, 1950). Based on the study of turbidites in the Alps in south-eastern France, a complete turbidity current event should include five sequences: TA (greywacke with graded bedding, and the bottom is provided with channel mold, ditch mold, and other scouring molds), TB (sandstone with parallel bedding), TC (siltstone with small ripple cross and deformation beddings), TD (siltstone and silty mudstone with a horizontal texture), and TE (massive mudstone) (Bouma, 1962). With the development of deep-water sedimentation, the concept of sandy debris flow and the established slope gravity-driven sediment retransportation models have been increasingly accepted (Shanmugam et al., 1994, 2000; Lai et al., 2019). These models have proven helpful in studying deep-water sediments and have significantly improved the understanding of sediment gravity flow sediments. In gravitational flow research, the Bouma sequence proposed by Bouma in vertical research and the fan model proposed by Walker's (1978) in-plane research are crucial. Walker believes the turbidite fan is formed in deep-water, comprising an upper, middle, and lower fan. Like conventional fans, he believes that the

upper fan primarily develops fan root deposits with channels, the middle fan also has channels and similar channel overflow sediments, and the lower fan primarily comprises some sheet-like sediment transformed by water flow. After the Walker fan theory was put forward, numerous scholars have discovered gravitational flow deposits that are not in a fan-shaped state, such as point provenance, line provenance, and multiple provenance deposition patterns (Reading and Richards, 1994). Consequently, the theoretical system of turbidity current has been established and perfected. Before and after the 21st century, many scholars disagreed on the understanding of the turbidite current theory, including the Bouma sequence and various fan models, denied the theoretical system of turbidity current, and proposed a new viewpoint of developing large-scale bulk transport deposition and sandy debris flow in deep-water environments (Shanmugam, 1996). To sum up, the development of gravitational flow sedimentation research has experienced recognition of turbidity currents in the 1950s, the widespread recognition of the Bouma sequence and various fan models from the 1960s to 1980s, being questioned in the 1990s (Shanmugam, 2002), and finally proposing the concept of sandy debris flow and the corresponding slope deposition model in the 21st century.

Sediment gravity flow is the primary mechanism for transporting sediments to deep-water basins (Normark and Piper, 1972; Mulder and Alexander, 2001). Based on the hydrodynamic mechanism, the gravity transport process of underwater sediments was divided into elastic, elastic plastic, plastic, and viscous flows (Dott, 1963). Based on the particle support mechanism, gravity flow was divided into turbidity current, debris flow, particle flow, and liquefied sediment flow (Middleton and Hampton, 1976). Some scholars divided slope gravity flow into sliding, collapse, debris flow, and turbidity current (Shanmugam, 2013). The classification scheme was based on the gravity flow formation process and its fluid properties in each stage. The classification scheme was straightforward and clear and had strong applicability. Fluid properties and sedimentary characteristics were considered, and core, experiment, and field investigation verifications were conducted with a high reference value. Research has found that the gravity flow types in China's continental lake basin were divided into block carrier and turbidity current. The former was subdivided into sliding rock, collapse rock, and debris flow. Turbidity current is turbidite and was described in detail from the aspects of the formation process, sediment concentration, flow pattern, mechanics rheological characteristics support, sedimentary mechanism, and identification marks (Pan et al., 2013). The gravity flow in the Chang 6 member of the Yanchang Formation of the Upper Triassic in the Baibao area, Ordos Basin, was studied, the gravity flow sedimentary model in the study area was established, and the facies zones were divided. From the perspective of production practice, it was divided into three zones: collapse root, middle part, and basin plain, and promising exploration targets were proposed (Zou et al., 2009). Located in eastern China, the Bohai Bay Basin is a large oil-bearing Paleogene intracontinental fractured basin (Hu et al., 1986; Li, 1986). The basin's deep-water gravity flow sandstone is a vital oil reservoir (Zhu et al., 1991). Due to its economic importance, Chinese scholars have extensively studied the Bohai Bay Basin's gravity flow channel. In the research in 2010, the exploration focus was on the delta in the Dongying Sag. The gravity flow in the Huanghua depression of the Bohai Bay Basin was divided into turbidity current, liquefaction flow, particle flow, and sandy debris flow (Xian et al., 2012). Some researchers proposed end debris flow deposition when studying the delta front gravity flow in the Dongying Sag (Wang, 1991). For a long time, the oil and gas exploration of the deep-water gravity flow sand body in the Dongying Sag mostly applies the Bouma sequence and the submarine fan facies model, and the end debris flow deposition has not received attention (Hou et al., 2002; Wang et al., 2003a; Yao et al., 2004; Wang et al., 2011). In recent years, as the contribution of gravity flow reservoirs to productivity has increased, some researchers have studied gravity flow in the Dongying Sag. The concept of the slope-shifting turbidite fan was proposed. It was considered that the slope-shifting turbidite fan was a lacustrine flooding period when the base level rose, and lake water waves and floods eroded and scoured the sedimentary sand bodies in the delta front and plain, resulting in the sedimentary sand body migration along the slope of the edge of the lake basin and the formation of redeposition in the deeper lake area (Wang et al., 2003b). By using fine sequence stratigraphic comparison, we can identify the vertical superposition relationship of multistage gravity flow sedimentary systems and reveal the temporal and spatial configuration relationship of gravity flow sand body deposition in different parts of the slope zone (Gomberg et al., 2021). A better exploration effect was obtained.

In recent years, some gravity flow sand bodies with obvious differences between sedimentary characteristics and turbidity currents have been found in oil and gas explorations (Chen et al., 2014; Yang et al., 2020). Their sedimentary characteristics, identification marks, control factors, and distribution laws were unclear. Consequently, the gravity flow sand bodies have achieved specific results in actual oil and gas explorations and encountered many problems. Therefore, there is a need to establish a more applicable and predictive sedimentary model to guide the gravity flow sand body's oil and gas exploration in the Dongying Sag. Based on the summary and analysis of previous studies, two problems in the research on the delta and gravity flow in $E_2S_3^2$ in the Dongying Sag occurred. First, the sedimentary charac-

teristics and identification marks of the collapse-gravity flow in the delta front of $E_2S_3^2$ in the study area were unclear; therefore, they negatively affected the application of the gravity flow reservoir. Second, the plane shape and internal structure of different gravity flow sand bodies in the study area were also unclear; therefore, there was a need to establish an advanced application and predictive sedimentary model. These problems severely restricted further oil and gas exploration of gravity flow reservoirs in the study area. This study systematically solved these problems and established an accurate sedimentary model and distribution characteristics of the sedimentary system. The sedimentary model is critical to enrich and improve the theory of gravity flow and guide the exploration and development of gravity flow oil and gas in the Dongying Sag.

2 Study area

2.1 Geological setting

The Bohai Bay Basin is in the south-east of the Eurasian plate and the central area of the interaction and intersection of the three tectonic domains of the Pacific, Tethys, and paleo–Asian Oceans. It is a Mesozoic Cenozoic superimposed composite basin in the North China Plate. The Dongying Sag is a secondary negative structural unit of the Jiyang depression in the Bohai Bay Basin in the south-east of the Jiyang depression (Zhang et al., 2020). It is adjacent to the Gaoqing uplift to the west, the Chenjiazhuang Binxian uplift to the north, the Qingtuozi uplift to the east, and the Luxi and Guangrao uplifts to the south (Lu et al., 2013). The study area is east of the Dongying Sag, and faults control its north and south sides. It is adjacent to the central uplift belt bound by the Xianhe fault to the north and connected to the southern slope bound by the Chenguanzhuang Wangjiagang fault terrace to the south. The study area is 39 km long from east to west and 34 km wide from north to south, covering approximately 1326 km^2 (Fig. 1).

2.2 Sedimentological setting and sequence stratigraphy

The structural activity of the Tanlu fault controls the Dongying Sag, which has experienced three primary stages of structural development: the early Eocene rifting, the late Oligocene synrift intensive rifting, and the postrifting subsidence from the Miocene to the present. According to the study area's drilling records, the Cenozoic strata developed successively from the bottom to the top in the Paleogene Kongdian Formation (E_1k), Shahejie Formation (E_2s), Dongying Formation (E_3d), Neogene Guantao Formation (Ng), and Minghuazhen Formation (Nm) (Yuan et al., 2015). The E_2s can be further divided into four subsections (Fig. 2): the Sha4

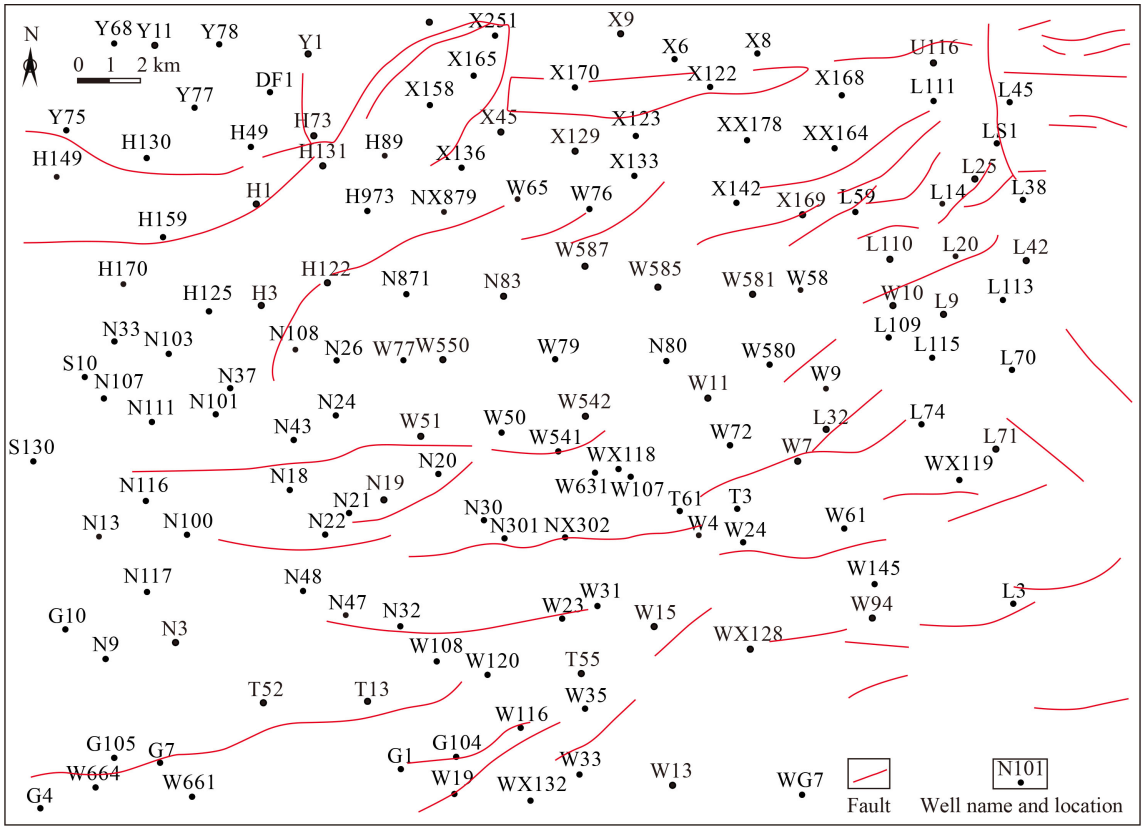

Fig. 1 Location of the study area.

section (E_2s_4) at the bottom and the Sha1 section (E_2s_1) at the top. The study horizon is $E_2S_3^2$. The lower part of $E_2S_3^2$ is characterized by thick dark gray mudstone interbedded with calcite mudstone and thin calcite sandstone, whereas the upper part is characterized by thick massive antirhythmic fine sandstone interbedded with thin gray and gray-green mudstone.

In the $E_2S_3^2$ period, the Dongying delta's primary sand body accumulated into the Niuzhuang Sag. By analyzing the termination pattern of seismic reflection in the Niuzhuang Sag, the Shahejie Formation between the T4 reflection axis at the top of $E_2S_3^2$ and the T6 reflection axis at the bottom of $E_2S_3^2$ is the developed sedimentary stratum (Fig. 3(a)). During the sedimentary period of $E_2S_3^2$, a large-scale Dongying delta developed, advancing south-east to north-west and the delta's scope gradually expanded from morning to night. Therefore, $E_2S_3^2$ in the Niuzhuang Sag is divided into a T-R sequence—two system tracts of rapid lake transgression and regression are developed, divided into six (Z6, Z5, Z4, Z3, Z2, and Z1) sequence groups from the bottom to the top, corresponding to the 6-stage delta sand bodies in the study area (Fig. 3(b)). The transgressive system tract corresponds to sequence set Z6, and the regressive system tract includes sequence sets Z5–Z1 (Sajiadi et al., 2015).

3 Materials and methods

3.1 Materials

Through the observation and analysis of 14 coring wells in $E_2S_3^2$ in the Dongying Sag and logging means, core photographs, lithology data, and other research data, the characteristics of gravity flow lithology and lithofacies combinations were analyzed to deepen the understanding of gravity flow lithology, sedimentary structure, and sedimentary microfacies (Table 1). According to the observed coring data of gravity flow wells, the stratum of the coring well section is $E_2S_3^2$, with a depth of 2192.0–3344.5 m and a core length of 618.97 m.

The mudstone in $E_2S_3^2$ primarily comprises mudstone and sandy mudstone divided into six sublayers (Table 2). The Z1 sublayer is mudstone, siltstone, and middle sandstone, and the Z2, Z4, and Z5 sublayers are mudstone, fine sandstone, and medium sandstone. The Z3 sublayer is mudstone, siltstone, and fine sandstone, and the Z6 sublayer is mudstone and coarse sandstone.

The lithostratigraphic assemblage of $E_2S_3^2$ in the study area was sand mudstone interbedding, the roundness of clastic particles was mostly secondary ridge, the sorting was medium–good, the weathering degree was medium,

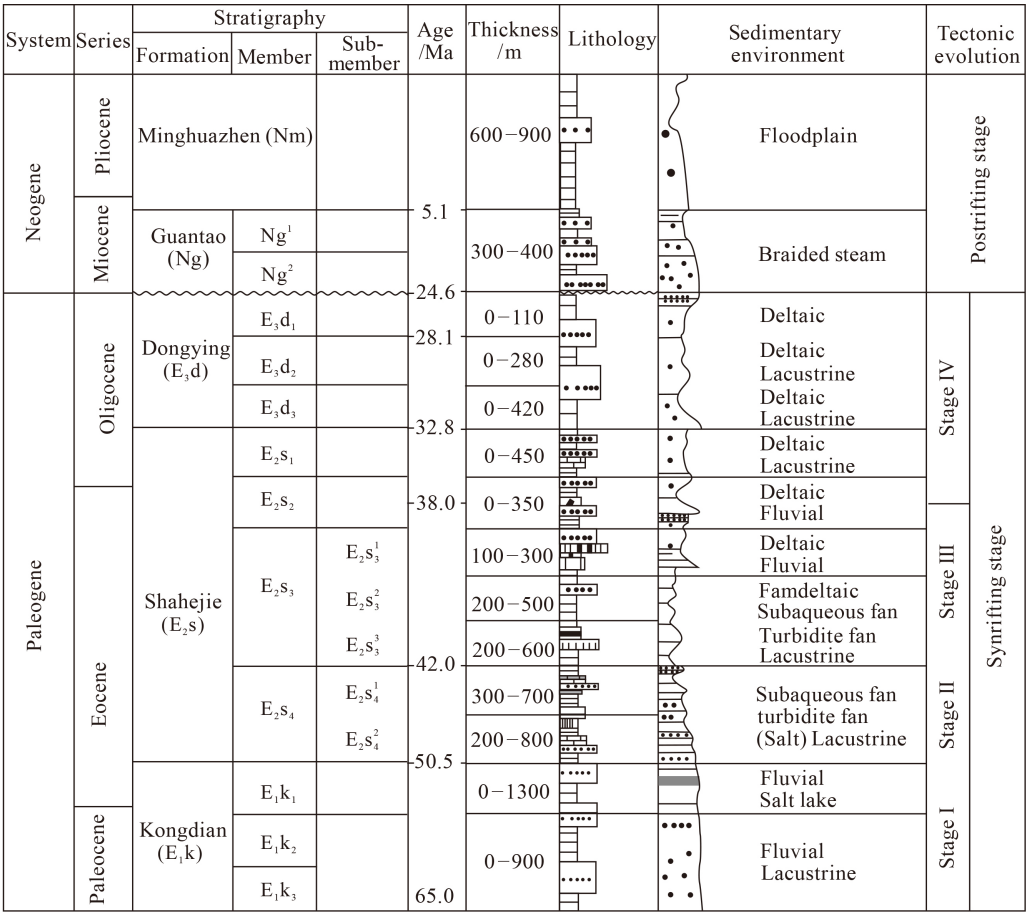

Fig. 2 Generalized stratigraphy of the Dongying Sag, showing the lithology, sedimentary environment, and the tectonic evolution.

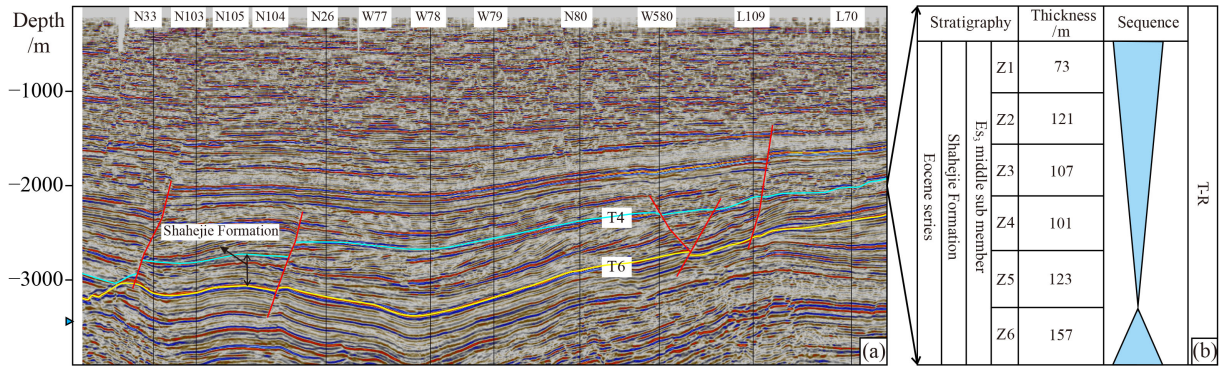

Fig. 3 Sequence stratigraphy of the study area. (a) Seismic interpretation profile; (b) sequence stratigraphic division.

Table 1 Coring data of gravity flow well

Serial number	Well number	Top depth/m	Bottom depth/m	Horizon	Coring length/m
1	N48	2865	2904.5	$E_2S_3^2$	39.2
2	N100	3027	3035		0.4
3	N101	2192.3	2199.9		61
4	N116	3097	3116.9		14.6
5	N117	2495	2867.3		13.1
6	H130	2243.3	3269.9		103
7	H159	2949	3344.5		71.2
8	G12	2379.00	3325.60		15.60
9	N116	3097.00	3116.90		14.56
10	N20	3001.17	3079.11		63.93
11	W108	2192.00	2711.19		13.30
12	N22	2734.50	2739.40		4.90
13	N33	3028.00	3226.00		187.68
14	N111	3008.90	3301.98		16.50

Table 2 Lithology data of each small layer of 60 Wells in $E_2S_3^2$

Sublayer	Mudstone thickness/%	Siltstone thickness/%	Fine sandstoneThickness/%	Medium sandstone thickness/%	Coarse sandstone thickness/%
Z1	44.7	25.9	8.5	13.6	7.3
Z2	50.0	0	22.4	27.6	0.0
Z3	44.8	16.4	28.7	10.1	0.0
Z4	51.2	8.4	16.4	24.0	0.0
Z5	56.1	3.8	20.1	20.0	0.0
Z6	57.9	7.5	9.3	0.0	25.3

porous cementation, particle support, and the particle size was 0.06–0.25 mm, reflecting the characteristics of rapid deposition (Table 3). The study area's overall structural maturity of sandstone was slightly poor–medium, close to the provenance.

3.2 Methods

This study analyzed the petrological characteristics, sedimentary structural characteristics, and logging facies characteristics of the gravity flow fan of the delta and gravity flow system of $E_2S_3^2$ in the Dongying Sag, Bohai Bay Basin, according to the analysis and test data, core data, and logging data, and investigated the sedimentary characteristics of gravity flow lithofacies and lithofacies assemblage characteristics. The study clarified the sedimentary type of gravity flow. The lithologic characteristics, grain size characteristics, sedimentary structure, and lithofacies combinations of different gravity flows were analyzed and summarized. Finally, the typical identification marks of different genetic gravity flow sand bodies in the delta front were defined.

Table 3 Statistics of structural maturity of some clastic rocks in $E_2S_3^2$

Well No.	Horizon	Sample number	Depth/m	Main particle size/mm	Sorting	Roundness	Support mode	Cementation type	Weathering degree
G12	$E_2S_3^2$	4	2460.8	0.25–0.50	Medium	Secondary edge	Particle	Pore	Medium
G12	$E_2S_3^2$	2	2462.9	0.13–0.25	Good			Pore	
N117	$E_2S_3^2$	3	2517	0.13–0.50	Medium			Crystal stock	
W120	$E_2S_3^2$	1	2003.1	0.13–0.50	Medium			Pore	
W120	$E_2S_3^2$	5	2003.1	0.25–0.50	Medium-Good			Pore	
N117	$E_2S_3^2$	4	2863	0.06–0.13	Medium			Pore	
S130	$E_2S_3^2$	2	3035	0.13–0.25	Medium			Crystal stock-Pore	
S130	$E_2S_3^2$	3	3041.66	0.13–0.25	Poor-Medium			Crystal stock-Pore	
N116	$E_2S_3^2$	4	3097	0.13–0.25	Medium			Pore	
N116	$E_2S_3^2$	2	3109.3	0.13–0.25	Medium			Pore	

The target well's core with gravity flow development in the Dongying Sag was selected and finely described using the core physical profile and scanning image to classify the sedimentary characteristics of gravity flow sediments in the study area. Combined with the sedimentary characteristics and identification marks of different gravity flow sedimentary types, and by analyzing gravity flow single-well facies and profile facies, the differences in gravity flow sedimentary types and vertical sequences at different distribution positions were clarified to characterize their distribution characteristics.

Rock samples at 30 depths were collected from 14 coring wells, and log data were collected from 60 wells. Using these rock samples, numerous microscopic characterization experiments, such as thin-section analysis, scanning electron microscopy, and X-ray diffraction analysis experiments, were conducted using optical or electron microscopy. Copious particle size data of the primary coring wells were analyzed and combined with other particle size parameter data, and the particle sizes in the particle size data were used to draw the probability accumulation curve. Then, the CM value was obtained from the probability accumulation curve to draw the CM diagram. The core characteristics, sedimentary structure, sedimentary and microfacies characteristics, depositional system distribution characteristics of the delta, and the gravity flow in $E_2S_3^2$ in the Dongying Sag are systematically studied. The delta and gravity flow sedimentary model was established based on studying the sedimentary characteristics, distribution law, and internal structure of different gravity flow sand bodies in the study area.

4 Sedimentary characteristics

4.1 Lithologic characteristics

The lithology of $E_2S_3^2$ in the Dongying Sag was primarily mudstone, fine sandstone, medium sandstone, and siltstone. The mudstone content was 50.8% (Fig. 4(a)), and the color was mostly gray, dark gray, and green-gray. The fine sandstone content was 17.6%, and the medium sandstone content was 15.9%. The color was mostly gray and gray-white, and gravelly sandstone was rare. The primary sandstone types were lithic arkose and arkose (Fig. 4(b)), in which the average quartz content was 44%, and feldspar was 32%.

4.2 Grain size characteristics

The probability accumulation curve of the delta front is primarily two-stage and transition-stage (Fig. 5(a)). The overall slope-of-jump was large, reflecting a strong hydrodynamic force and good sand body sorting. The OP/PQ section representing traction and drainage is primarily shown on the CM diagram. The slope-shifting fan sand body's grain size probability accumulation curve was primarily three-stage and two-stage. Compared with the delta front, the overall slope-of-jump sub reduced, the overall content of the suspension sub increased, the grain size interval span was large, and the sorting worsened (Fig. 5(b)). In the CM diagram, the OP and PQ segments representing traction and drainage are represented. The QR segments representing gravity flow significantly increased, with particle size characteristics of traction and gravity flows (Liu et al., 2016). The wide and gentle upward arch type and the single section type dominated the probability accumulation curve of turbidite (Fig. 5(c)). The particle size characteristics of its CM diagram are turbidite type dominated by QR (Fig. 5(d)), reflecting typical progressive suspended sedimentation. The turbidite's C value increased in proportion to the M value, and the C value changed accordingly with the M value. Therefore, part of the figure is parallel to the C = M baseline.

In summary, the slope-shifting fan has the grain size characteristics of traction and gravity flows, where the sliding and collapse were only the displacement of the semiconsolidated delta front sand body. The sedimentary components changed a little and showed increasing

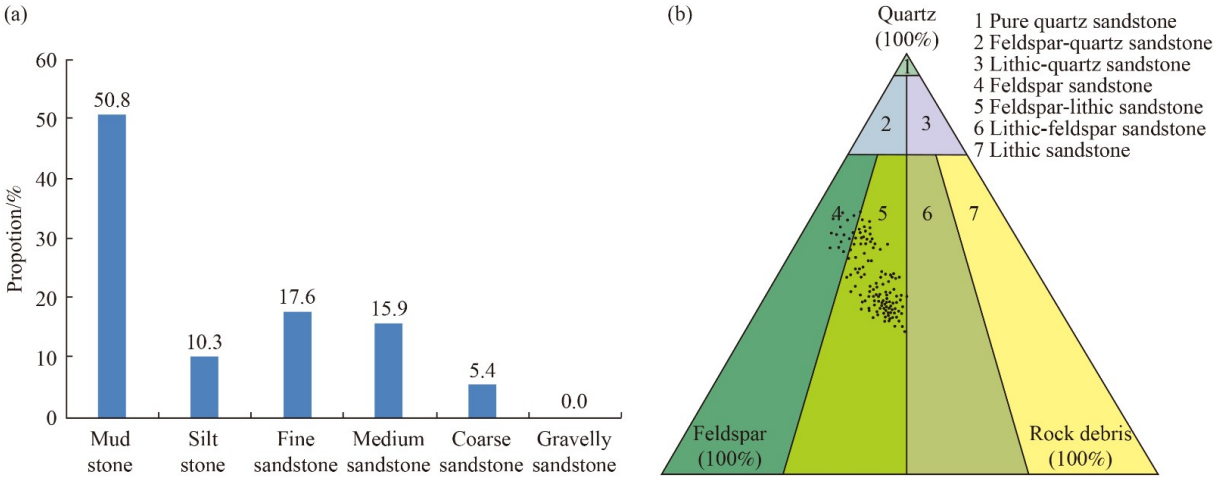

Fig. 4 Rock types and major compositions. (a) Lithologic histogram; (b) sandstone type map.

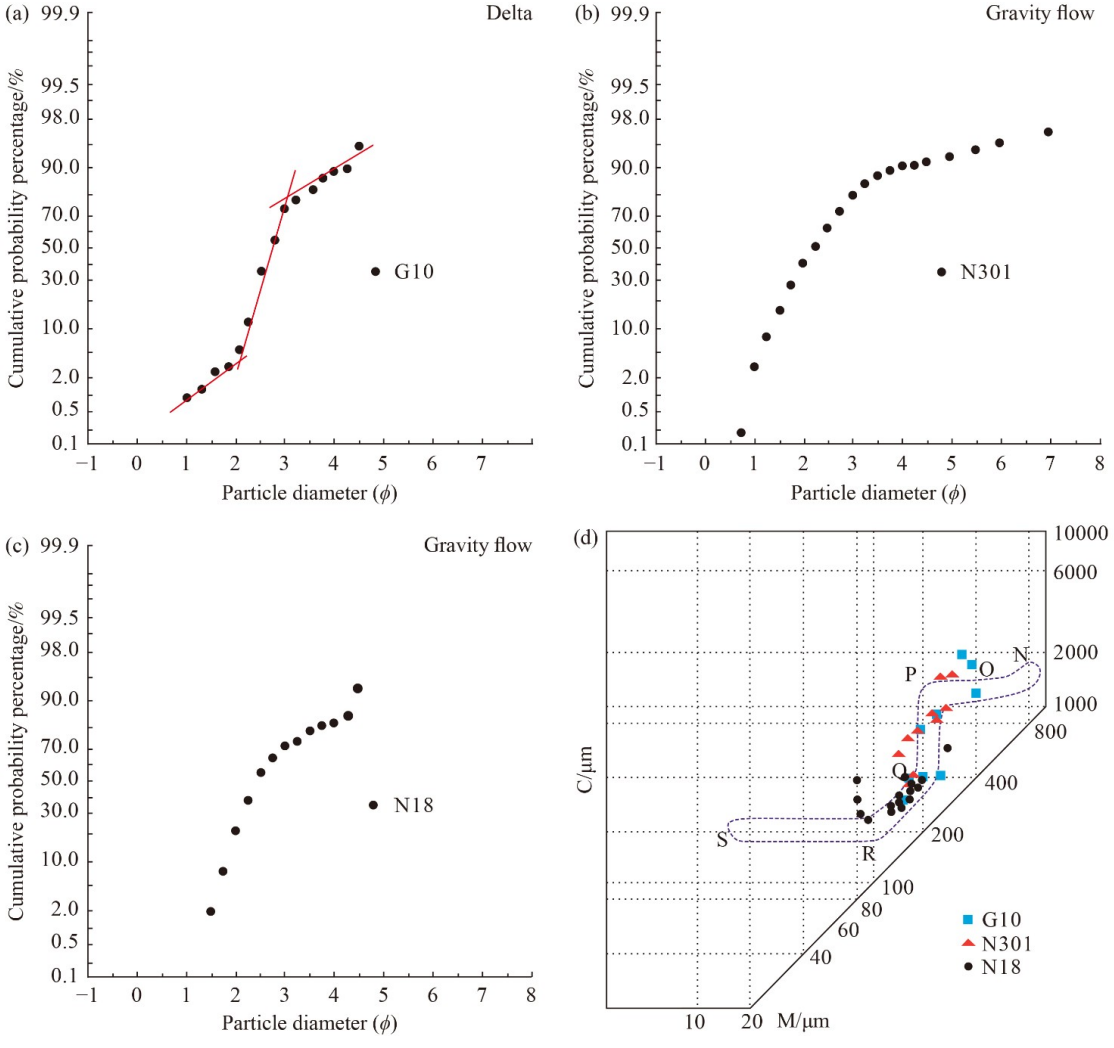

Fig. 5 Grain size cumulative probability curve and C–M diagram of sandstone.

traction and drainage characteristics. With the increase in the turbidity degree, it gradually transformed into gravity flow, and the grain size characteristics of debris flow were closer to turbidite.

4.3 Characteristics of gravity flow sedimentary structures

The core observations show that under the trigger of specific external conditions, the sediment slides down

under the action of gravity along the flat slip surface, and no obvious deformation occurs. Sedimentary structures were common, such as deformed bedding (Fig. 6(a)) and ball pillow structures (Fig. 6(b)).

Collapse is the product of a synsedimentary deformation structure in the sediment due to the combined action of its gravity and rotational shear force when the delta front sediment moves on the concave slip surface after instability. Sedimentary structures were common, such as deformation bedding (Fig. 6(c)), wrapping bedding (Fig. 6(d)), and flame structures (Fig. 6(e)) (Yang et al., 2015).

When the sliding and collapse deposits moved forward under the action of gravity and its components along the slope, they gradually developed into debris flow due to the continuous mixing of surrounding water media, and many sedimentary structures occurred, such as tear debris (Figs. 6(f) and 6(g)).

Turbidity current is a Newtonian fluid, which does not

Fig. 6 Sedimentary structure. (a) N30-2879.20 m, Deformation bedding; (b) N48-2896.66 m, Ball pillow structure; (c) N103-3069.45 m, Deformation bedding; (d) H130-3227.90 m, Wrapped bedding; (e) N22-3207.10 m, Flame structure; (f) N101-3216.90 m, Mudstone tear debris; (g) N30-2883.70 m, Mudstone tear debris; (h) N33-3077.00 m, Bouma sequence ACE; (i) YX331-2680.80 m, Bouma sequence BCDE.

have any yield strength. Once an external force acts on it, it moves. As long as the external force is not zero, the turbidity current does not stop moving. The debris flow continues to move forward, and the sediments are further diluted under the action of the surrounding water to finally form a turbidity current. Sedimentary structures were common, such as Bouma sequences ACE (Fig. 6(h)) and BCDE (Fig. 6(i)).

4.4 Single-well facies analysis

Well H159 (Fig. 7) is represented by sliding–collapse, debris flow, and some turbidity current deposits. The well's 2950–2960 m section primarily comprises sliding–

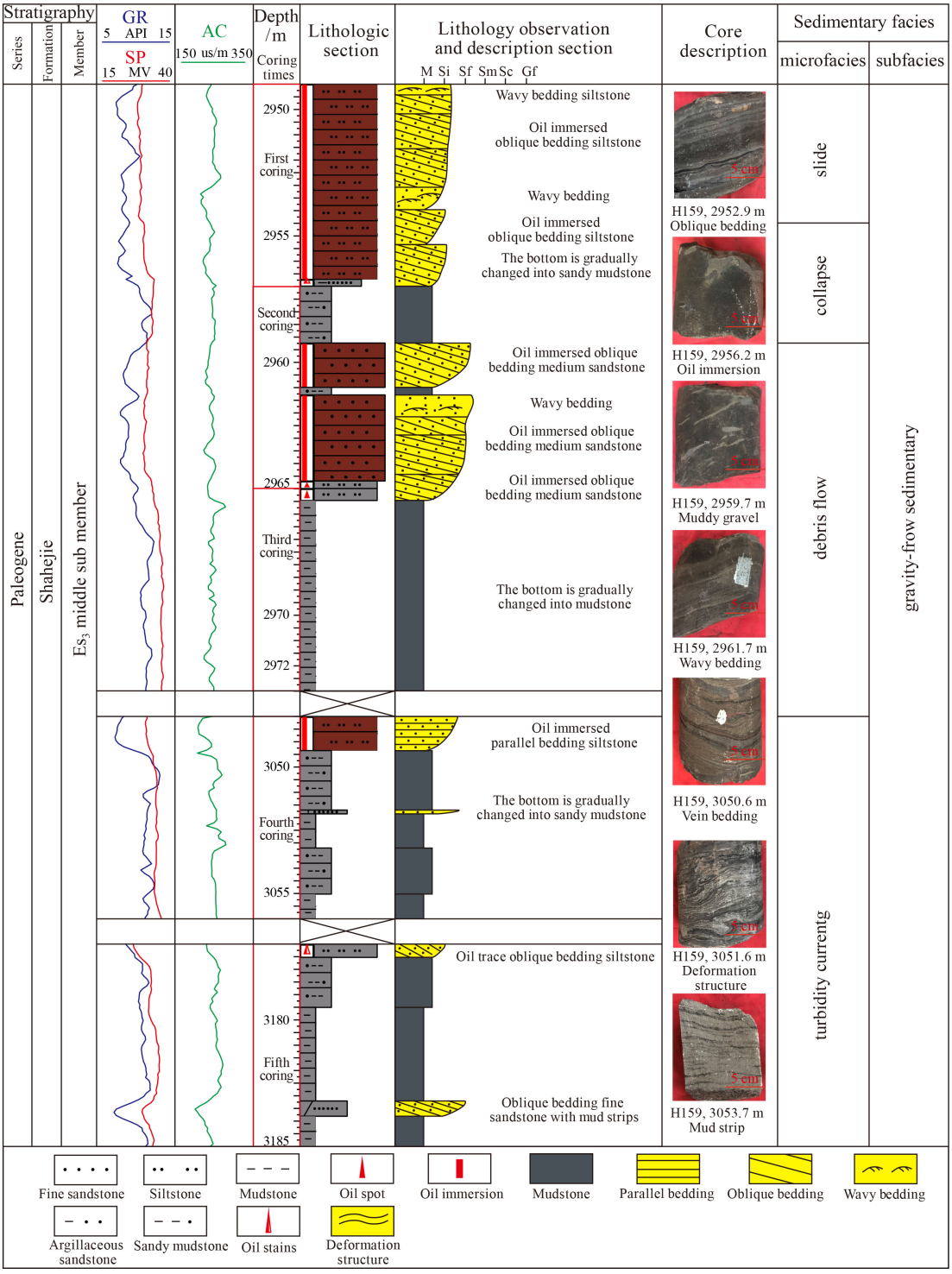

Fig. 7 $E_2S_3^2$ single well facies (Well H159).

collapse deposits and fine sandstone deposits, and internally developed undeformed underwater distributary channel (including retained deposits at the bottom of the channel) and collapse deformation structures.

At 2960–2968 m, it primarily comprises debris flow deposition, with the characteristics of multistage superposition. The lithology was siltstone and fine sandstone, the sand body was massive, and heterogranular rocks and rich mud gravel and mudstone tearing debris occurred.

It comprises turbidity current deposition at 3051–3057 m, with some thin sandy strips inside. Gravity flow sedimentation evolved from debris flow sedimentation to sliding–collapse sedimentation from the bottom to the top, reflecting the characteristics of reverse cycle sedimentation, which echoes with the continuous progradation facies of the Dongying delta.

4.5 Lithofacies characteristics

The study area was far from the provenance, the sedimentary rock types were moderately unified, and the sedimentary sequences were similar. It was challenging to distinguish the microfacies and rock types separately and to understand the relationship between different microfacies. Therefore, this study identified sedimentary microfacies according to the combination characteristics of lithofacies. Based on the specified lithofacies types, single and composite lithofacies models were established.

4.5.1 Single lithofacies

According to the characteristics of rock structure, bedding, and grain size in the study area, nine single lithofacies were divided into gravity flow facies. These lithofacies included clean massive sandstone (SCM), boulder bearing massive sandstone (SFC), positive progressive sandstone (SNG), corrugated crossbedding (siltstone) sandstone (SRC), crossbedding fine sandstone (SCB), deformed bedding argillaceous sandstone (MSDB), boulder bearing argillaceous sandstone (MSFC), deformed bedding sandy mudstone (SMDB), and boulder bearing massive mudstone (MMFC) (Fig. 8).

Lithofacies			Sedimentary structure	Corresponding core		Average thickness/m	Sedimentary facies
				Photo	Well & MD		
Scm	Fine sandstone / medium sandstone		Homogeneous, massive, visible carbon chips		N116 3014.5 m	0.42	Debris flow
Sfc	Fine sandstone/ medium sandstone		floating gravel, mud gravel, tearing debris,		N48 2880.6 m	0.72	Debris flow
Sng	Fine sandstone/ very fine sandstone		Positive progressive bedding		N33 3160.4 m	0.34	Turbidity current
Src	Very fine sandstone/ siltstone		Corrugated cross bedding		YX331 2682.8 m	0.40	Turbidity current
Scb	Fine sandstone		Cross bedding, visible anti rhythm		Y101 2891.7 m	1.03	Slide
MSdb	Argillaceous sandstone		Wrapped bedding, crumpled bedding		H130 3227.7 m	0.60	Collapse
MSfc	Argillaceous sandstone		Floating gravel, mud gravel, tearing debris,		N30 2873.5 m	0.56	Debris flow
SMdb	Sandy mudstone		Wrapped bedding		G10 2779.9 m	1.37	Collapse
Mmfc	Mudstone		Mud gravel, sandy mass, tearing debris		Y691 2694.1 m	1.57	Turbidity current

Fig. 8 Single lithofacies types.

4.5.2 Lithofacies combinations

According to the detailed observation and description of core samples, the combination relationship of typical lithofacies of gravity flow sedimentation in the study area was summarized. Nine single lithofacies were reorganized, and five lithofacies assemblages were identified. Combined lithofacies types included SCB-SCB, MSDB-MSDB, SCM-SFC, SFC-SCM, and SNG-SNG-SNG. These lithofacies assemblage types were consistent with the sedimentary facies types (Fig. 9).

4.6 Logging facies characteristics

Logging facies was first proposed in 1979, and it was considered to characterize the formation characteristics and distinguish it from other formations (Serra, 1984). The sedimentary facies were interpreted using a spontaneous potential curve as the primary method and the resistivity curve as the auxiliary method. Through analysis, the spontaneous potential logging curve of the target interval in the study area had four forms (Fig. 10).

The box curve (N117, H125, and S10) shows medium–low amplitude and toothed box types. The top and bottom of the curve were abrupt. The corresponding lithology was siltstone, fine sandstone, and sandstone, with a thin mudstone layer in the middle. It indicated that the material source supply was sufficient, the water flow energy was moderately stable, the curve was slightly toothed, and some fine layers contained mud, indicating that the water energy changed slightly. It often represented sublacustrine fan channels and channel sedimentation. The bell-shaped curve (N22, X139) was medium–high amplitude- and toothed-bell-shaped, and the bottom of the curve was abrupt. The corresponding lithology was sandstone and pebbly sandstone. With the increase in the argillaceous content in sandstone, the curve amplitude gradually transitioned to mudstone from the bottom to the top. Therefore, the curve shape was bell-shaped from the bottom to the top, indicating that the sedimentary condition in geological history was the decrease in sediment supply. It might also have been that the flow energy gradually weakened from the bottom to the top, representing the lateral migration of the river channel. Funnel-shaped curves (L109, N301, and XX178) were medium–low amplitude funnel-shaped and toothed funnel-shaped. The top of the curve was abrupt, and the corresponding lithology was siltstone and sandstone. The curve's shape was the opposite of the bell-shaped curve. The mud content decreased gradually from the bottom to the top, and the sand content increased gradually, representing the distributary estuary deposition of the delta front.

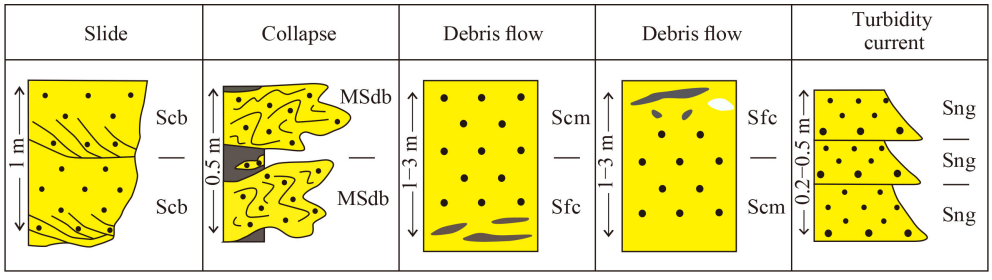

Fig. 9 Lithofacies combination types.

Sedimentary type		SP			GR			Logging facies characteristics
Delta front		L109	XX178	N301	L109	XX178	N301	SP: Inverted funnel type GR: Inverted funnel type
Slope fan	Slide / Collapse	N117	H125	S10	N117	H125	S10	SP: Funnel box composite GR: Box tooth type
	Debris flow	N32	Y691	N30	N32	Y691	N30	SP: Funnel type GR: Dentate funnel type
Turbidite	Turbidity current	G104	N22		G104	N22		SP: Finger or bell GR: Toothed bell

Fig. 10 $E_2S_3^2$ gravity flow logging facies characteristics.

Finger curves (H146, G104) showed a medium–high amplitude finger shape, and the corresponding lithology was fine sandstone and siltstone, with a thickness of 2–3 m, often representing fan end deposition.

4.7 Sedimentary facies and microfacies characteristics

Slope fan deposition refers to various sediments or sedimentary rocks formed by sediment gravity flow, which can form in any environment with sediment gravity flow. This study focused on the gravity flow deposition in the delta front sedimentary environment of the Dongying Sag in the faulted lake basin (Wang, 2005). Through core observations and simulations of the front slope's sediment process path, the gravity flow sedimentation of $E_2S_3^2$ in the Dongying delta was integrated into slope fan deposition and turbidite deposition. Sliding, collapse, and debris flow microfacies were developed in the slope-shifting fan, and turbidity current microfacies were developed in turbidites.

4.7.1 Sliding microfacies

As the delta extends into the lake, the delta front sediments thicken, forming a unique front slope. Many factors affected the internal stability of the late delta sediments deposited on the slope. After the internal stability was destroyed, the slope sediments underwent shear failure and moved along the slope to the lake basin's center—a sediment retransportation process. The front sediments slide along the slope, forming a unique sliding structural feature. The lithology was gray medium fine sandstone with a thin layer of siltstone. Crossbedding, wavy bedding, parallel bedding, and other shallow water sedimentary structures could be seen. The spontaneous potential curve was toothed or slightly toothed box, bell, box combination, and finger, with medium amplitude (Fig. 11).

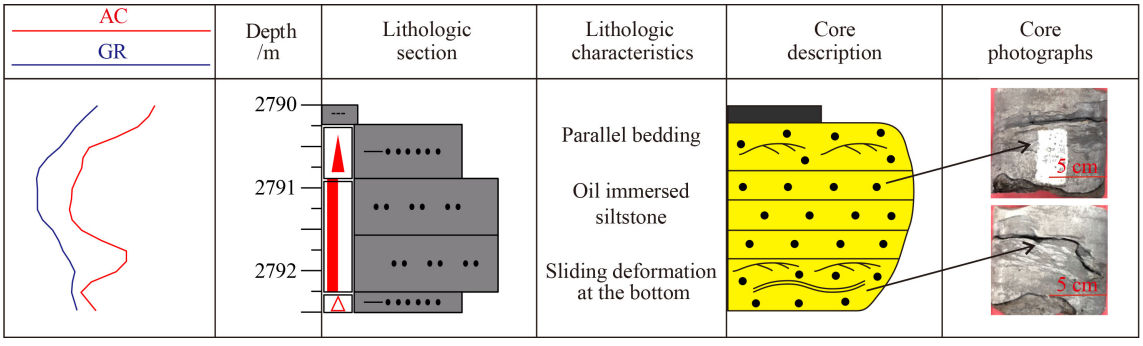

Fig. 11 Characteristics of sliding microfacies (Well H130).

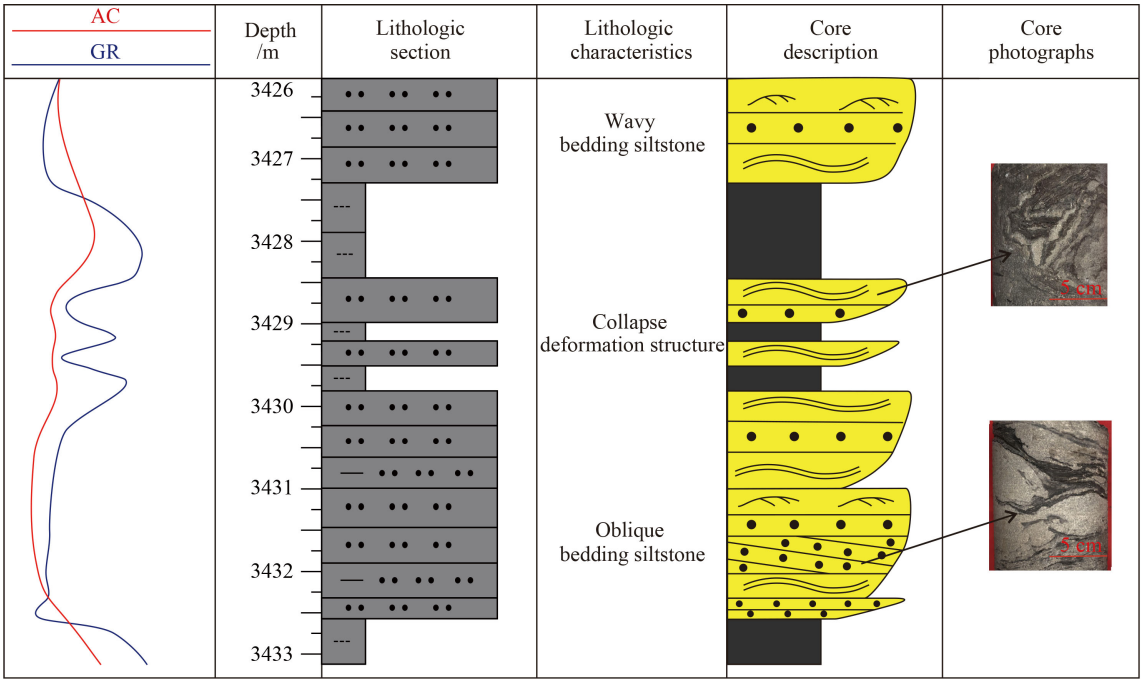

Fig. 12 Characteristics of collapse microfacies (Well W78).

4.7.2 Collapse microfacies

The front sliding deposition and the previous sliding on the underwater uplift slope formed the collapse. Collapse is the effect of soft sediments sliding down the slope or flowing along the layer caused by gravity, water flow, and vibration. The sliding speed of the collapse is fast and sudden, and the sliding speed is small, even peristaltic. Pore pressure frequently occurs in collapse and sliding. The lithology was primarily fine siltstone sandstone. Sandstone liquefaction, wrapped structure, heavy load mold structure, collapse structure, flame structure, lenticular sand body, and other sedimentary structures could be seen. The spontaneous potential curve was toothed or slightly toothed box, bell, box combination, and finger, with medium amplitude (Fig. 12).

4.7.3 Debris flow microfacies

During the early sedimentary period of $E_2S_3^2$ in the Dongying delta, the climate changed from dry to wet, the rain was abundant, and the material source supply was sufficient. Many complex sediments, such as mud, sand, and gravel flowed through the delta deposition and pushed into the lake until they accumulated in the deep lake semideep lake area, forming coarse debris flow deposits far from the shore. The lithology was primarily gravelly coarse sand, coarse sandstone, and medium sandstone. Massive structures, progressive bedding, wavy bedding, mudstone tearing debris, and other sedimentary structures could be seen. The spontaneous potential curve was primarily a box bell finger combination (Fig. 13).

4.7.4 Turbidity current microfacies

Compared with slope fan deposition, turbidity current sedimentary sand bodies were weakened in thickness and development scale. A turbidity current sedimentary sand body is a thin layer sand body formed in a deep lake sedimentary environment under the action of lake hydrodynamic force after the redeposition of the delta front's sand body. Its primary development characteristics are thin sand bodies in deep lacustrine sedimentary environments, and the Bouma sequence assemblage is CDE. The lithology was thick dark gray silty mudstone with thin silty fine sandstone. The overlying sandstone frequently presents sedimentary structures, such as parallel bedding, crossbedding, and corrugated crossbedding. The spontaneous potential curve was toothed or slightly toothed box- and finger-shaped, and the amplitude was medium (Fig. 14).

5 Discussion

5.1 Sedimentary system distribution characteristics

From the distribution characteristics of a sedimentary system, the Qingtuozi uplift to the north-east and the Guangrao uplift to the south-east are the primary provenances. Progradational delta and gravity flow deposits developed in $E_2S_3^2$ in the study area (Zhao et al.,

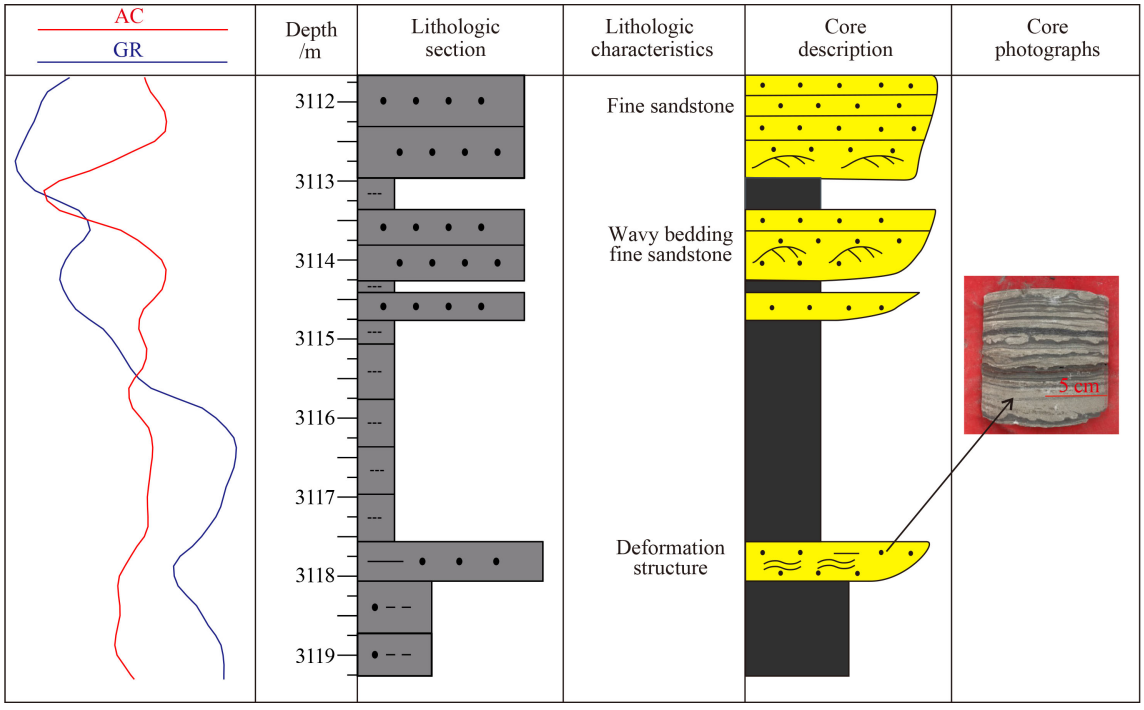

Fig. 13 Microfacies characteristics of debris flow (Well N116).

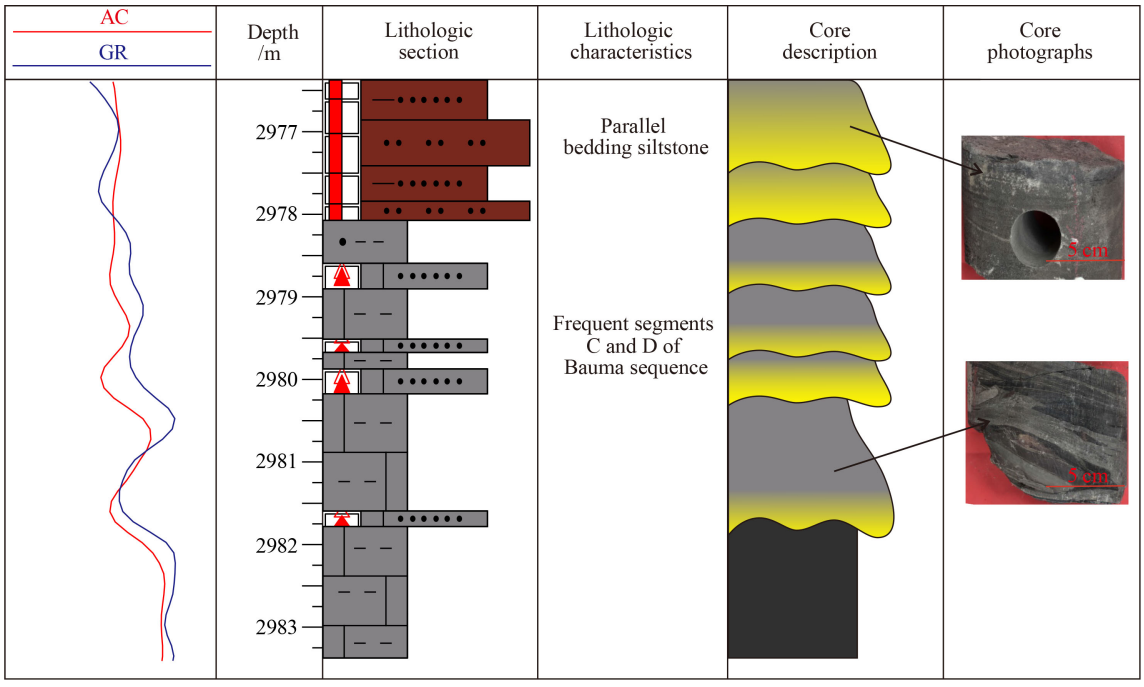

Fig. 14 Microfacies characteristics of turbidity current (Well Y922).

2011). During the sedimentary period of $E_2S_3^2$, the sediment source supply was sufficient. With the continuous sediment source supply from the raised area to the lake basin and the gradual reduction in the paleo-water depth, the flow characteristics in the south and steep in the north of the slope migrated to the lake basin in the west, controlling the temporal and spatial distribution of delta progradation units (Fig. 15).

Due to the obvious delta progradation in the study area, especially in the front of the delta, a fast deposition rate occurred. When the slope increased to a specific angle, many sediments carried by the delta progradation unit became unstable under gravity along the slope (Cao and Liu, 2007). Loose sediments accumulated in the front slope zone. Under the influence of earthquakes, waves, faults, and other actions, delta front sliding deposition developed, followed by delta front collapse. With the sliding and collapse of the front sand body, the sediments gradually reached the deep to semideep lake sedimentary environments. Under the influence of lake hydrodynamic forces, it gradually deposited in the lake basin far from the front, forming turbidity current depositions. Whether in the gentle slope zone of the Dongying Sag or the central depression of the lake basin, turbidity current deposits were primarily distributed in the predelta facies. With the continuation of sedimentation, the delta gradually developed to the center of the lake basin.

During the sedimentary period of the Z4–Z6 small layers in $E_2S_3^2$, the sand body development reached its peak, its thickness and scale were the largest, and it gradually thinned from south-east to north and north-west. During the sedimentary period of the Z1–Z3 small layers in $E_2S_3^2$, the provenance in the south gradually disappeared, whereas the provenance in the south-east was the primary provenance supply, and a large-scale delta plain deposition developed (Fig. 16).

In conclusion, the primary sedimentary types in $E_2S_3^2$ were deep to semideep lacustrine subfacies, gravity flow, delta front, and delta plain. The provenance is primarily from the south and east, and the eastern provenance gradually advances westward from the bottom to the top. The southern provenance is more abundant in the early sedimentary period of $E_2S_3^2$, especially in the sedimentary period of the Z6 layer in $E_2S_3^2$, and the gravity flow related to the front deposition is the largest. After that, the source supply gradually decreased, the fore-edge of the lake retreated to the south, and the gravity flow scale decreased accordingly.

5.2 Sedimentary model

According to the regional sedimentary background, the sedimentary characteristics and spatial distribution characteristics of sand bodies of different genesis, the analysis of sedimentary facies of single and connected wells in key wells, and the evolution law of gravity flow sedimentation, the gravity flow sedimentation model of $E_2S_3^2$ in the Dongying delta was established from a process sedimentology perspective (Fig. 17) (Xian et al., 2016).

According to previous studies in China and abroad (Lu, 2012; Liao et al., 2013), during the sedimentary period of $E_2S_3^2$, the rapidly accumulated sand body in the delta front of the study area was retransported under its action

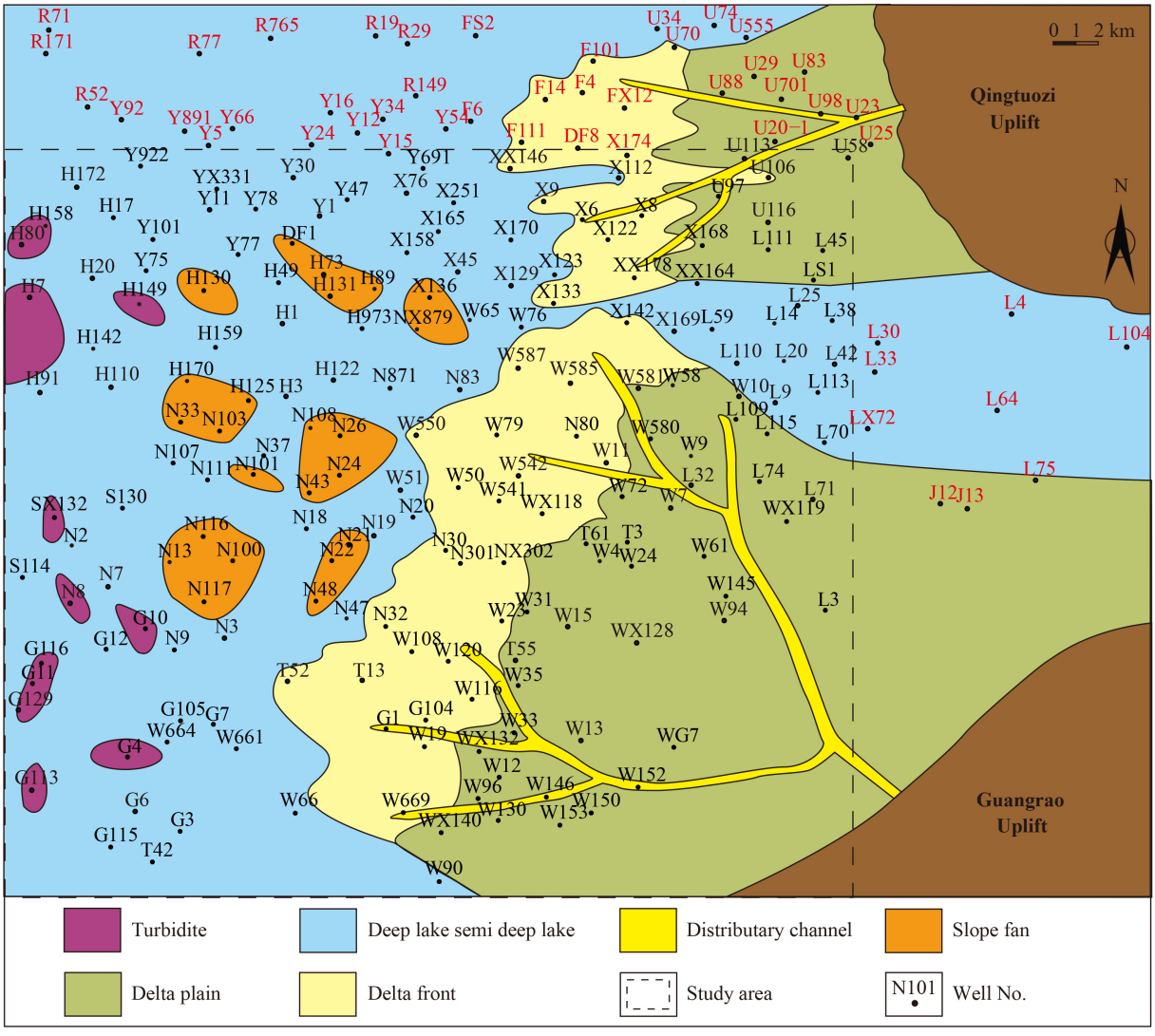

Fig. 15 The sedimentary facies of $E_2S_3^2$ in the Dongying Sag.

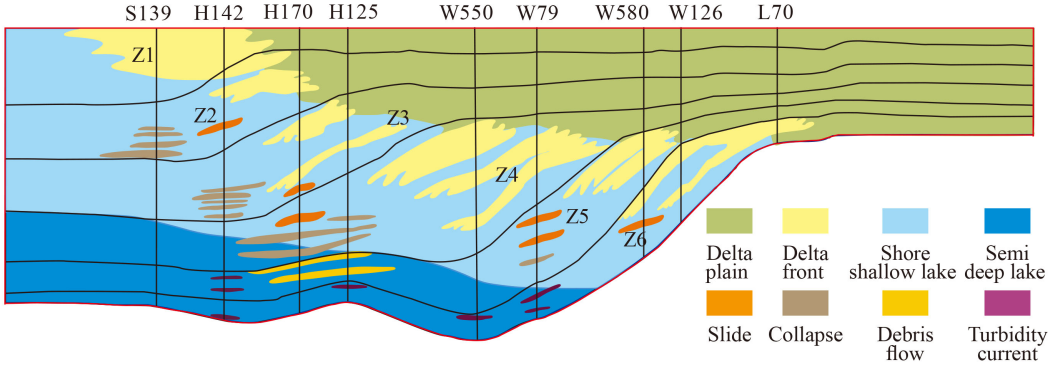

Fig. 16 Profile of sedimentary microconnected wells of wells (L70-W126-W580-W79-W550-H125-H170-H142-S139).

mechanism or an earthquake trigger mechanism. From the basin's slope to the center, the retransported sand experienced an evolution process of sliding–collapse–debris flow-turbidity current. The sediments first underwent translational movement and developed sliding sedimentation. With the continuous transportation of sediments and the continuous mixing of external water bodies, the pore pressure in the sediments increased and became muddy. Various syngenetic deformation structures developed under gravity to form a collapse sedimentary combination. The collapse deposits gradually evolved into debris flow deposits with plastic rheological

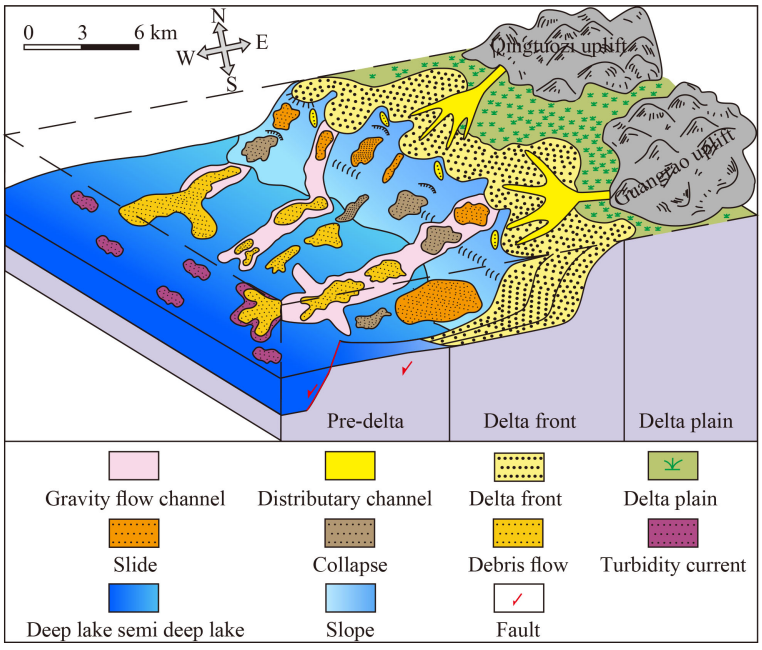

Fig. 17 Sedimentary model of $E_2S_3^2$ delta-gravity flow system in the Dongying Sag.

properties with the continuous transportation of blocks and the dilution and transformation of the surrounding fluids. Here the matrix content in sandstone was low; it was primarily the original mud in the sandstone, which floated in the sandstone under the support mechanism of debris flow dispersion pressure, matrix strength, and upward buoyancy, forming a debris flow lithofacies with low matrix strength. With the increase in block transportation distance, deep-water mud was gradually mixed. Due to the difference in sand mud yield strength and parent rock lithology, the mud mixed in the deep-water was torn and arranged disorderly or in layers, forming debris flow lithofacies with high matrix strength. With the increase in transportation distance, the top of the debris flow transformed into turbidity current, forming a debris flow-turbidity current-mixed lithofacies association until it was finally transformed into turbidity current.

6 Conclusions

1) The grain size of sandstones of different sedimentary types differs. The cumulative probability curve of the delta front sand body is a three-segment type, whereas the slope displacement fan is mostly a two-segment type. Turbidite is a wide and gentle upward arch shape that cannot be segmented.

2) The sedimentary facies was gravity flow, and its microfacies included sliding, collapse, debris flow, and turbidity current, divided into nine single lithofacies and five lithofacies association types. The sand bodies of different sedimentary types have corresponding typical logging curve combination characteristics.

3) During the sedimentary period of $E_2S_3^2$, the southeast provenance supply was sufficient. Wave action and its gravity were affected by fault activities, and the rapidly accumulated delta sand bodies in the study area slipped and collapsed, forming different types of gravity flow deposits. With the continuous advancement of the river delta, the gravity flow sand body gradually disappears in the late $E_2S_3^2$ and transits to delta plain deposition.

Acknowledgments This work was supported by the Natural Science Foundation of Shandong Province (No. ZR2020MD035); the National Natural Science Foundation of China (Grant Nos. 51504143 and 51674156).

References

Bouma A H (1962). Sedimentology of Some Flysch Deposits: a Graphic Approach to Facies Interpretation. Amsterdam, New York: Elsevier Publishing Company

Cao Y, Liu H (2007). Discussion on the relationship between distribution of fluxoturbidite and depositional slope of delta in lacustrine basin. Geol Rev, 53(4): 454–459 (in Chinese)

Chen X, Jiang Z, Du W, Wang J, Zhang Y (2014). Origin of depositional cycles and their influence on oil-bearing sandstone of Dongying Delta in Mid-Es3 Dongying Depression. Acta Sediment Sin, 32(2): 344–353 (in Chinese)

Dott R H (1963). Dynamics of subaqueous gravity depositional processes. AAPG Bull, 47: 104–128

Forel F A (1885). Les ravins sous-lacustres des fleuves glaciaires. Comptes Rendus de l'Académie des Sciences Paris, 101: 725–728

Gomberg J, Ariyoshi K, Hautala S, Johnson H P (2021). The finicky nature of earthquake shaking-triggered submarine sediment slope

failures and sediment gravity flows. J Geophys Res Solid Earth, 126(10): e2021JB022588

Hou M, Tian J, Chen H, Chen X, Xiao H, Qiu G, Jia G (2002). Turbidite fan characters of the intermediate section of Member 3 of Shahejie Formation in Niuzhuang depression of Dongying area. J Chengdu U Techn, 29(5): 506–510 (in Chinese)

Hu J, Xu S, Tong X (1986). Formation and distribution of complex petroleum accumulation zones in Bohai Bay Basin. Pet Explor Dev, 1: 1–8

Kuenen P H, Migliorini C I (1950). Turbidity currents as a cause of graded bedding. J Geol, 58(2): 91–127

Lai F, Li Z, Zhang T, Zhou A, Gong B (2019). Characteristics of microscopic pore structure and its influence on spontaneous imbibition of tight gas reservoir in the Ordos Basin, China. J Petrol Sci Eng, 172: 23–31

Li D (1986). Prospect of the composite megastructural oil and gas field in Bohai Gulf of China. Acta Petrol Sin, 7: 1–21

Liao J, Zhu X, Deng X, Sun B, Hui X (2013). Sedlimentary characteristics and model of gravity flow in Triassic Yanchang Formation of Longdong Area in Ordos Basin. Earth Sci Front, 20(2): 29–39

Liu X, Liu H, Song G, Jia G, Yang H (2016). Sedimentary characteristics and distribution pattern of the slope-shifting fan in the low-lying slope zone of Dongying Sag. Oil Gas Geol, 23(4): 1–10

Lu S, Chen G, Wu k, Feng D (2013). Tectonic feature and evolution mechanism of central anticline belt of Dongying Sag, Bohai Bay Basin. Petrol Geo & Experi, 35(3): 274–279 (in Chinese)

Lu Z (2012). Sedimentary characteristics and model of gravity flows in Yan 18 area of the steep slope in Dongying sag of Jiyang depression. Nat Gas Geosci, 23(3): 420–429

Middleton G V, Hampton M A (1976) Subaqueous sediment transport and deposition by sediment gravity flows. In: Stanley D J, Swift D P, eds. Marine Sediment Transport and Environmental Management. New York: Wiley, 197–218

Mulder T, Alexander J (2001). The physical character of subaqueous sedimentary density flows and their deposits. Sedimentology, 48(2): 269–299

Normark W R, Piper D J W (1972). Sediments and growth pattern of Navy deep-sea fan, San Clements Basin, California Borderland. J Geol, 80(2): 198–223

Pan S, Zheng R, Wei P, Wang T, Chen B, Liang S (2013). Deposition characteristics, recognition mark and form mechanism of mass transport deposits in terrestrial lake Basin. Lithologic Reserv, 25(2): 9–18 (in Chinese)

Reading H G, Richards M (1994). Turbidite systems in deep-water basin margins classified by grain size and feeder system. AAPG Bull, 78: 792–822

Sajiadi F, Hashemj H, Borzuee E (2015). Palynostratigraphy of the Nayband Formation, Tabas, Central Iran Basin: paleogeographical and paleoecological implications. J Asian Earth Sci, 111: 553–567

Serra O (1984). Fundamentals of Well-Log Interpretation: The Acquisition of Logging Data. Amsterdam: Elsevier Publishing Company, 1–35

Shanmugam G (1996). High-density turbidity currents: are they sandy debris flows? J Sediment Res, 66(1): 2–10

Shanmugam G (2000). 50 years of the turbidite paradigm (1950s–1999s); deep-water processes and facies models-a critical perspective. Mar Pet Geol, 17(2): 285–342

Shanmugam G (2002). Ten turbidite myths. Earth Sci Rev, 58(3–4): 311–341

Shanmugam G (2013). New perspectives on deep-water sandstones: implications. Pet Explor Dev, 40(3): 294–301

Shanmugam G, Lehtonen L R, Straume T, Syvertsen S E, Hodgkinson R J, Skibeli M (1994). Slump and debris-flow dominated upper slope facies in the Cretaceous of the Norwegian and northern North Seas (61°–67° N); implications for sand distribution. AAPG Bull, 78: 910–937

Walker R G (1978). Deep-water sandstone facies and ancient submarine fans: models for exploration for stratigraphic traps. Am Assoc Pet Geol Bull, 62: 932–966

Wang D (1991). The sedimentation and formation mechanism of lacustrine endogenic debris flow. Acta Geol Sin, 65(4): 299–316

Wang H, Zhou T, Song J, Miao X (2011). Recognition of sedimentary characteristics and its significance to petroleum geology the 3rd member of Shahejie Formation Paleogene western Dongying Depression. Geoscience, 25(4): 626–634 (in Chinese)

Wang J (2005). Sedimentary facies of the Shahejie Formation of Paleogene in Dongying Sag, Jiyang Depression. J Paleogeogr, 7(1): 45–58 (in Chinese)

Wang J, Han W, Yu J, Zheng J (2003a). Turbidity system in the third section of Shahejie Formation of Dongying Sag and its implications on petroleum prospecting. Acta Petrol Sin, 24(6): 24–29

Wang J, Jia G, Liu J, Li X (2003b). Discussion on the genesis model for turbidites of Es3 in Shinan area. Oil & Gas Recov Techn, 10(4): 8–10 (in Chinese)

Xian B, Wan J, Jiang Z, Zhang J, Li Z, Yu Y (2012). Sedimentary characteristics and model of gravity flow deposition in the depressed belt of rift lacustrine basin: a case study from Dongying Formation in Nanpu Depression. Earth Sci Front, 19(1): 121–135

Xian B, Wang L, Liu J, Lu Z, Li Y, Niu S, Zhu Y, Hong F (2016). Sedimentary characteristics and model of delta-fed turbidites in Eocene easterm Dongying depression. J China U Petrol (Natural Science Version), 40(5): 10–21 (in Chinese)

Yang T, Cao Y, Wang Y, Zhang S (2015). Types, sedimentary characteristics and genetic mechanisms of deep-water gravity flows: a case study of the middle submember in Member 3 of Shahejie Formation in Jiyang Depression. Acta Petrol Sin, 36(9): 1048–1059

Yang W, Wang Q, Song Y, Jiang Z, Meng W, Liu G, Zhang B (2020). New scaling model of the spontaneous imbibition behavior of tuffaceous shale: constraints from the tuff-hosted and organic matter-covered pore system. J Nat Gas Sci Eng, 81: 103389

Yao M, Zhong J, Guo J, Yang H, Liu J (2004). Turbidite characteristics of delta front for the 3rd Member of Shahejie Formation in Niuzhuang Sag, Jiyang depression. Geol J China U, 10(4): 624–633 (in Chinese)

Yuan G, Gluyas J, Cao Y, Oxtoby N H, Jia Z, Wang Y, Xi K, Li X (2015). Diagenesis and reservoir quality evolution of the Eocene sandstones in the northern Dongying Sag, Bohai Bay Basin, East China Mar Pet Geol, 62: 77–89

Zhang Y, Zhang X, Cao H, Zheng X, Wang J, Zhang J (2020). Paleogene lake deep water sedimentary facies in the northern zone of the Chezhen Sag, Bohai Bay Basin, China. J Petrol Explor Product Techn, 10(1): 4–14 (in Chinese)

Zhao W, Qiu L, Jiang Z, Chen Y, Liu J, Yang Y (2011). Distribution and evolution of sedimentary facies of the middle of the third member of Shahejie Formation, Paleogene System in Minfeng Sub-sag, Jiyang Depression. Acta Sediment Sin, 29(2): 5–10 (in Chinese)

Zhu X, Xiong J, Liu Z, Xin Q (1991). Axial gravity flow deposit in Dongpu Depression. J China U Petrol (Natural Science Version), 15: 1–9 (in Chinese)

Zou C, Zhao Z, Yang H, Fu J, Zhu R, Yuan X, Wang L (2009). Genetic mechanism distribution of sandy debris flows in terrestrial lacustrine basin. Acta Sediment Sin, 27(6): 1065–1075 (in Chinese)